Faraday Discussions

Energy-resolved and time-dependent unimolecular dissociation of hydroperoxyalkyl radicals (•QOOH)

Journal:	*Faraday Discussions*
Manuscript ID	FD-ART-01-2022-000008.R1
Article Type:	Paper
Date Submitted by the Author:	21-Jan-2022

Complete List of Authors:	BHAGDE, TRISHA; University of Pennsylvania School of Arts and Sciences, Chemistry Hansen, Anne; University of Pennsylvania School of Arts and Sciences, Chen, Shu-Guang; State Key Laboratory of Coordination Chemistry, School of Chemistry and Chemical Engineering, Collaborative Innovation Center of Advanced Microstructures, Nanjing University, Nanjing 210023, P. R. China, Walsh, Patrick; UPenn, chem Klippenstein, Stephen; Argonne National Laboratory, Chemistry Division Lester, Marsha; University of Pennsylvania, Department of Chemistry

SCHOLARONE™
Manuscripts

Energy-resolved and time-dependent unimolecular dissociation of hydroperoxyalkyl radicals (•QOOH)

Trisha Bhagde[1*], Anne S. Hansen[1*], Shuguang Chen[1], Patrick J. Walsh[1], Stephen J. Klippenstein[2], and Marsha I. Lester[1]

[1] Department of Chemistry, University of Pennsylvania, Philadelphia, PA 19104-6323, USA
[2] Chemical Sciences and Engineering Division, Argonne National Laboratory, Lemont, IL 60439, USA

Abstract

Hydroperoxyalkyl radicals (•QOOH) are transient intermediates in the atmospheric oxidation of volatile organic compounds and combustion of hydrocarbon fuels in low temperature (< 1000 K) environments. The carbon-centered •QOOH radicals are a critical juncture in the oxidation mechanism, but have generally eluded direct experimental observation of their structure, stability, and dissociation dynamics. Recently, this laboratory demonstrated that a prototypical •QOOH radical [$•CH_2(CH_3)_2COOH$] can be synthesized by an alternative route, stabilized in a pulsed supersonic expansion, and characterized by its infrared (IR) spectroscopic signature and unimolecular dissociation rate to OH radical and cyclic ether products. The present study focuses on a partially deuterated •QOOD analog $•CH_2(CH_3)_2COOD$, generated in the laboratory by H-atom abstraction from partially deuterated *tert*-butyl hydroperoxide, $(CH_3)_3COOD$. IR spectral features associated with jet-cooled and isolated •QOOD radicals are observed in the vicinity of the transition state (TS) barrier leading to OD radical and cyclic ether products. The overtone OD stretch ($2\nu_{OD}$) of •QOOD is identified by IR action spectroscopy with UV laser-induced fluorescence detection of OD products. Direct time-domain measurement of the unimolecular dissociation rate for •QOOD ($2\nu_{OD}$) extends prior rate measurements for •QOOH. Partial deuteration results in a small increase in the TS barrier predicted by high level electronic structure calculations due to changes in zero-point energies; the imaginary frequency is unchanged. Comparison of the unimolecular decay rates obtained experimentally with those predicted theoretically for both •QOOH and •QOOD confirm that unimolecular decay is enhanced by heavy-atom tunneling involving simultaneous O-O bond elongation and C-C-O angle contraction along the reaction pathway.

* Equal contributions

Introduction

The oxidation of volatile organic compounds (VOCs) in the troposphere and low temperature combustion of hydrocarbon fuels (<1000 K) proceed by analogous radical chain reaction mechanisms.[1-3] The VOC or fuel typically reacts with hydroxyl (OH) radicals by hydrogen abstraction from an alkyl group or addition to an unsaturated site to form carbon-centered radicals R•. The R• radicals rapidly react with atmospheric O_2 to form organic peroxy radicals ROO•.[4] The ROO• radicals can then isomerize via intramolecular H-atom transfer to form transient hydroperoxyalkyl radicals •QOOH, composed of a hydroperoxide group (–OOH) and a new carbon radical center •Q, which have generally eluded direct experimental detection.[5-7] The transient •QOOH radicals are a critical juncture in the oxidation mechanism leading to several possible outcomes: isomerization via internal H-shift back to ROO•, unimolecular decay to release OH and a cyclic ether (chain propagating), elimination of HO_2 to form an alkene (effectively chain terminating because HO_2 is not very reactive), and bimolecular addition of a second O_2 to generate oxygen-centered peroxy radicals •OOQOOH. The •OOQOOH radicals can undergo analogous isomerization and decomposition steps, yielding additional OH radicals (chain branching).[8] Alternatively, repeated cycles of H-transfer (ROO• $\rightarrow$ •QOOH) and O_2 addition (•QOOH $\rightarrow$ •OOQOOH) can create more highly oxidized molecules that drive formation of secondary organic aerosols (SOAs) in the atmosphere.[9-12]

A schematic reaction pathway for production and unimolecular decay of the prototypical carbon-centered •QOOH radical transiently formed in the oxidation of isobutane or other branched hydrocarbons is illustrated in Figure 1.[6, 13, 14] Recently, this laboratory demonstrated that this prototypical •QOOH radical could be generated and stabilized under jet-cooled and isolated conditions.[6] Specifically, the 2-hydroperoxy-2-methylprop-1-yl (•$CH_2(CH_3)_2COOH$) radical was produced in the laboratory by H-atom abstraction from *tert*-butyl hydroperoxide (TBHP), and characterized through its infrared (IR) spectroscopic signature and unimolecular decay dynamics to OH products.[6, 7] Prior experimental studies of this •QOOH radical under thermal conditions had detected only its products, specifically OH radicals and 2,2 dimethyl epoxide (DMEPOX), and •OOQOOH radicals formed upon addition of O_2.[14, 15] These prior studies also provided temperature- and pressure-dependent kinetic measurements for the appearance of OH products.

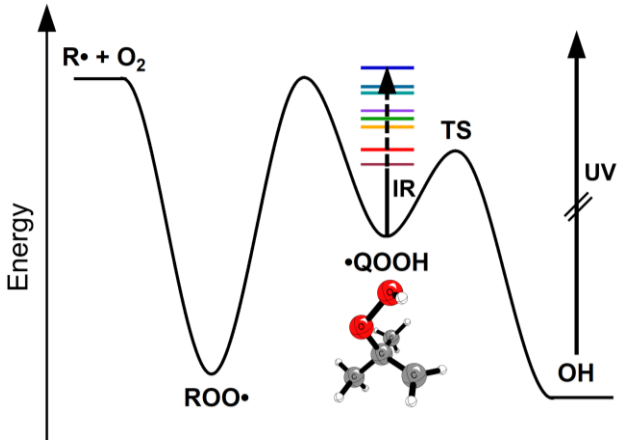

Figure 1. Schematic reaction pathway for production and unimolecular decay of the carbon-centered hydroperoxyalkyl radical intermediate (•QOOH) in oxidation of isobutane or other branched hydrocarbons. An alkyl radical (R•), typically formed by OH abstraction or addition, reacts with O_2 to produce an alkylperoxy radical (ROO•), which can isomerize via an intramolecular H-shift to produce •QOOH. IR spectral features of jet-cooled and stabilized •QOOH radicals have recently been observed at energies that lie below and above the transition state (TS) barrier leading to OH radical and cyclic ether products.[6, 7] In the current study, partially deuterated •QOOD is vibrationally activated, which induces unimolecular decay and leads to OD radical products that are detected by UV laser-induced fluorescence.

Recently, this laboratory conducted IR pump – UV probe measurements to obtain IR action spectra and time-resolved unimolecular decay rates for the •QOOH radical.[6, 7] The experiments utilized IR pump excitation to vibrationally activate •QOOH at energies in the vicinity of the transition state (TS) barrier leading to OH and DMEPOX products. A UV probe laser then detected the OH radical products resulting from unimolecular decay by UV laser-induced fluorescence (LIF). Scanning the IR pump laser provided a distinctive spectral fingerprint of the •QOOH radical from 2950 to 7050 cm^{-1}.[7] The observed transitions are associated with overtone OH and CH stretch transitions, combination bands involving OH or CH stretch and a lower frequency mode, and fundamental OH and CH stretch transitions. The •QOOH transitions observed in the IR action spectra are identified by comparison with anharmonic vibrational frequency calculations[7] and, in most cases, readily distinguished from IR transitions of the TBHP precursor.[16-18]

Importantly, the IR activation provides sufficient energy for the jet-cooled •QOOH radicals to surmount or tunnel through the TS barrier leading to OH and cyclic ether products. As a result, the energy-resolved and time-dependent evolution of the •QOOH radicals to OH (v=0, N) products yield microcanonical energy-dependent unimolecular decay rates $k(E)$ for •QOOH in the vicinity of the TS barrier. These direct time-domain measurements revealed unimolecular decay rates ranging from $3.2 \pm 1.0 \times 10^6$ s^{-1} (and corresponding lifetime, $\tau = 309 \pm 96$ ns) at 3579.5 cm^{-1} to $\geq 2.6 \pm 0.5 \times 10^8$ s^{-1} ($\tau \leq 3.8 \pm 0.8$ ns; laser limited) at 6971.5 cm^{-1}.[6]

Energy-dependent microcanonical rates $k(E)$ are exquisitely sensitive to the properties of the TS barrier that leads to unimolecular reaction.[6, 19-21] For •QOOH, the experimental rates $k(E)$ are both more rapid and extend to lower energy than anticipated based on a prior exploration of the TS barrier involving a high-level focal point analysis that yielded a zero-point corrected dissociation barrier of 12.0 kcal mol^{-1}.[13] Rather, substantially higher-level electronic structure methods were required to obtain a more reliable barrier of 10.3 kcal mol^{-1} and imaginary frequency (763i cm^{-1}) at the TS, along with associated rovibrational properties at stationary points along the reaction coordinate.[6] The theoretical analysis revealed that the minimum energy pathway is composed of the simultaneous elongation of the O-O bond and contraction of the C-C-O angle, leading to OH radical and cyclic ether products. Subsequent statistical Rice–Ramsperger–Kassel–Marcus (RRKM) rate calculations[22] that utilized the combined reduction in the TS barrier height and imaginary frequency resulted in excellent agreement with experimental rate measurements over a wide range of energies from 10 to 20 kcal mol^{-1}, and demonstrated that heavy atom tunneling significantly enhances (two-fold) the unimolecular decay rates.[6] The experimentally measured and theoretically validated microcanonical rates $k(E)$ also enabled reliable extension using a fully *a priori* method[23] to obtain the pressure-dependent thermal unimolecular rate constants $k(T,P)$ for a prototypical •QOOH,[6] which are in excellent accord with prior kinetic studies of $k(T,P)$ based on the of appearance of OH products.[14, 15] The thermal unimolecular rate constants $k(T,P)$ are generally used in global chemical models of oxidation in atmospheric and combustion environments.[24, 25]

A prior observation of a resonantly stabilized •QOOH derived from oxidation of 1,3-cycloheptadience by Savee et al. utilized photoionization detection.[5] The resonance stabilization increased the stability of •QOOH and significantly increased the barrier (ca. 30 kcal mol^{-1}) for its unimolecular decomposition to OH products. The latter is ca. three-fold greater than TS barriers of 10-12 kcal mol^{-1} predicted for a wide range of •QOOH radicals,[26] including the prototypical •QOOH investigated here.

The present study expands our experimental and theoretical exploration of the microcanonical unimolecular decay rates for •QOOH upon partial deuteration of the hydroperoxyl group (•QOOD). Partial deuteration shifts the overtone OH/D stretch ($2\nu_{OH/D}$) and other vibrational mode(s) to lower frequencies, providing a new spectroscopic window on •QOOD and its microcanonical unimolecular decay rates. Partial deuteration results in changes of the IR spectrum as well as the rovibrational properties of the •QOOD reactant and TS, requiring a small zero-point energy correction to the TS barrier. Comparison of the experimental and computed rate(s) for •QOOD provide further validation of the high-level electronic structure calculations of the TS barrier and reaction pathway for this prototypical

•QOOH/D intermediate. In addition, it enables further examination of the importance of heavy atom tunneling in the unimolecular decay of the carbon-centered •QOOH/D radical.

Methods

Partially deuterated *tert*-butyl hydroperoxide [$(CH_3)_3COOD$, TBDP, ca. 93% deuteration on the OOH moiety] is synthesized as described in Supplementary Information (SI, Figures S1 – S2). Partially deuterated peroxyalkyl •QOOD radicals [2-deuteroperoxy-2-methylprop-1-yl, ($•CH_2(CH_3)_2COOD$)] are generated in an analogous manner as that demonstrated recently to produce •QOOH.[6] TBDP vapor is entrained in a gas mixture of Cl_2 (0.25%), He (ca. 25%), and Ar (ca. 75%) at 40 psi and pulsed through a solenoid valve with an affixed quartz capillary reactor tube into a vacuum chamber. Photolysis of Cl_2 near the exit of the capillary using the 355 nm output of a Nd:YAG laser (EKSPLA or Continuum 8000, ca. 5 mJ pulse^{-1}, 10 Hz) generates Cl atoms, which abstract a H-atom from one of the methyl groups of TBDP.[2] This produces •QOOD radicals that are collisionally stabilized and subsequently cooled in the supersonic jet expansion to a rotational temperature of ca. 10 K.[27, 28] The gas mixture is intersected by counter-propagating, spatially overlapped, and focused tunable IR-pump and UV-probe laser beams ca. 1 cm downstream in the collision-free regime of the expansion. The tunable IR pump radiation is generated from a KTP-based OPO/OPA (LaserVision, ca. 3 mm, 0.9 cm^{-1} bandwidth, 10 – 30 mJ/pulse, 5 Hz, Δt_{IR} = 2.8 ± 0.1 ns Gaussian pulse width) pumped by a Nd:YAG laser (Continuum Surelite EX) and the UV probe radiation is derived from a frequency-doubled Nd:YAG pumped dye laser (Continuum 7020 and ND6000, ca. 5 mm, ca. 3 mJ/pulse, 10 Hz, Δt_{UV} = 3.0 ± 0.1 ns Gaussian pulse width). IR activation of •QOOD generates OD $X^2\Pi_{3/2}$ (v=0) products that are probed by UV laser-induced fluorescence (LIF) on the OD $A^2\Sigma^+ – X^2\Pi_{3/2}$ (1,0) $Q_1(3.5)$ transition. Further details of the experimental methods are provided in Supplementary Information (SI).

The present study on •QOOD utilizes the high-level electronic structure calculations of the TS barrier region recently obtained for unimolecular decay of •QOOH, specifically geometries and harmonic vibrational frequencies calculated for •QOOH at the CCSD(T)-F12/cc-pVDZ-F12 level of theory coupled with higher level composite energies.[6] For •QOOD, harmonic vibrational frequencies of the reactant and TS are similarly computed at the CCSD(T)-F12/cc-pVDZ-F12 level of theory in Molpro.[29] The anharmonic vibrational frequencies and IR absorption intensities are evaluated for optimized B2PLYP-D3/cc-pVTZ geometries using second-order vibrational perturbation (VPT2) theory as implemented in Gaussian16.[30] XSEDE resources[31] are utilized for the anharmonic frequency calculations. Energies presented herein are obtained at the ANL0F level of theory,[32] as described previously,[6] and are anharmonic zero-point energy (ZPE) corrected unless otherwise stated. The ANL0F method includes basis set, CCSDT(Q) and other high-level corrections to the CCSD(T)-F12/cc-pVDZ-F12//B2PLYP-D3/cc-pVTZ within a focal-point like composite scheme. The energy-dependent unimolecular decay

rates, $k(E)$, for •QOOD are calculated using statistical RRKM theory.[22] The calculations are analogous to those carried out previously for •QOOH using the Master Equation System Solver (MESS).[33] The harmonic and anharmonic frequencies for •QOOD are summarized in Table S1.

Results and Discussion

The experimental search to identify IR transitions of partially deuterated •QOOH (•QOOD) under jet-cooled and stabilized conditions was guided by anharmonic vibrational frequencies and IR intensities computed using VPT2. The calculations indicate that the overtone OH stretch ($2\nu_{OH}$), combination band involving OH stretch and OOH bend ($\nu_{OH} + \delta_{OOH}$), and fundamental OH stretch will be shifted to significantly lower frequencies upon partial deuteration, as listed in Table 1 and illustrated in Figure 2. Specifically, the overtone OH/D stretch ($2\nu_{OH/D}$) is predicted to shift from 6984 cm^{-1} in •QOOH to 5201 cm^{-1} in •QOOD with greater than 2-fold loss in intrinsic intensity. The $\nu_{OH/D} + \delta_{OOH/D}$ transition is computed to shift from 4880 cm^{-1} in •QOOH to 3630 cm^{-1} in •QOOD, again with a 2-fold drop in predicted intensity for an already weak combination band. Finally, the fundamental OH/D stretch ($\nu_{OH/D}$) is predicted to shift from 3580 cm^{-1} in •QOOH to 2647 cm^{-1} in •QOOD, once again with nearly 2-fold loss in intensity. Moreover, the fundamental OD stretch (ν_{OD}) of •QOOD shifts significantly below the TS barrier for dissociation to OD products, precluding detection by IR action spectroscopy. The frequencies and intrinsic intensities of other vibrations of •QOOD are expected to be essentially unchanged from those in •QOOH. Thus, the experiments focused primarily on observation of the overtone OD stretch ($2\nu_{OD}$) of •QOOD predicted at 5201 cm^{-1}.

Table 1. Comparison of the observed IR transitions (cm^{-1}) with calculated (B2PLYP-D3/cc-pVTZ) anharmonic frequencies (cm^{-1}) and intensities (km mol^{-1}) for •QOOH and •QOOD using VPT2.[6, 7]

Transition	Observed Frequency		Calculated Frequency (Intensity)	
	•QOOH	•QOOD	•QOOH	•QOOD[b]
$2\nu_{OH/D}$	7015.5[a]			
	6971.5	5198.1	6984 (4.8)	**5201 (2.0)**
$2\nu_{CH_2}$	6187.0		6209 (0.3)	6209 (0.3)
$2\nu_{CH_3}$	5932.0		5942 (0.4)	5942 (0.4)
			5921 (0.3)	5921 (0.3)
$\nu_{OH/D} + \delta_{OOH/D}$	4879.0		4880 (0.6)	**3630 (0.3)**
$\nu_{CH_2} + \delta_{HCH}$	4534.0	4534.0	4562 (0.9)	4562 (1.0)
$\nu_{OH/D}$	3597.8[a]			
	3579.5		3580 (19)	**2647 (11.9)**
ν_{CH_2}	3025.0		3049 (21)	3049 (20.0)
ν_{CH_3}	2985.5		3000 (20)	3000 (20.0)

a: Observed feature attributed to $2\nu_{OH}$ transition of •QOOH2 and/or •QOOH3 conformers with a combined estimated population of 15%.

b: Bold indicates calculated transitions that change upon partial deuteration.

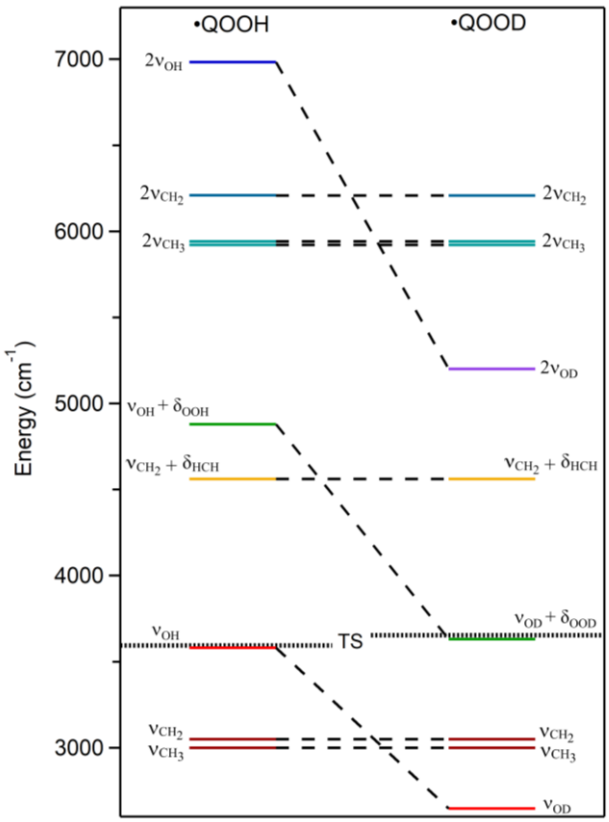

Figure 2. Comparison of calculated (B2PLYP-D3/cc-pVTZ) anharmonic frequencies using VPT2 for •QOOH and •QOOD radicals, •$CH_2(CH_3)_2COOH/D$. Vibrations associated with the partially deuterated OOD moiety show a substantial decrease in frequency. The horizontal black dotted lines represent the TS barriers, computed to be 10.3 kcal mol^{-1} for •QOOH and 10.5 kcal mol^{-1} for •QOOD, associated with the unimolecular dissociation of •QOOH/D to OH/D products.[6, 7]

A spectral search revealed the $2\nu_{OD}$ transition of •QOOD centered at 5198.1 cm^{-1}, which is shifted only 3 cm^{-1} to lower energy than that predicted theoretically. The IR-UV time delay was set at 50 ns, consistent with the predicted rapid dissociation to OD products (see below) that were detected by LIF on the A-X (1,0) $Q_1(3.5)$ transition. Scans across the 5170 to 5245 cm^{-1} region revealed no additional features, which might originate from higher energy conformers (•QOOD2 and/or •QOOD3) theoretically predicted to lie at 5219 and 5224 cm^{-1} (Table S2). In addition, the $2\nu_{OD}$ transition of TBDP, theoretically predicted at 5229 cm^{-1} (Table S2), is not observed, which would require IR multiphoton dissociation to release OD products utilized for detection in IR action spectroscopy.[17, 34, 35]

The rotational band contour for the overtone OD stretch of •QOOD ($2\nu_{OD}$) at 5198.1 cm^{-1} is consistent with a single isolated transition spanning ca. 15 cm^{-1}, as shown in Figure 3. The simulation is performed with PGOPHER[36] using a rotational temperature of 10 K along with computed rotational constants, the OPO bandwidth, and Lorentzian broadening of 1.7 cm^{-1}, the latter of which is consistent with rapid intramolecular vibrational energy redistribution (IVR) on a few picosecond timescale, although some

power broadening cannot be excluded. The homogeneous broadening washes out any detail of the rotational structure or transition type. The rotational band contour for the overtone OD stretch of •QOOD ($2\nu_{OD}$) is similar to that observed for the fundamental OH stretch of •QOOH (ν_{OH}) at 3579.5 cm^{-1}, but differs considerably from the overtone OH stretch of •QOOH ($2\nu_{OH}$) at 6971.5 cm^{-1} as shown in Figure 3.

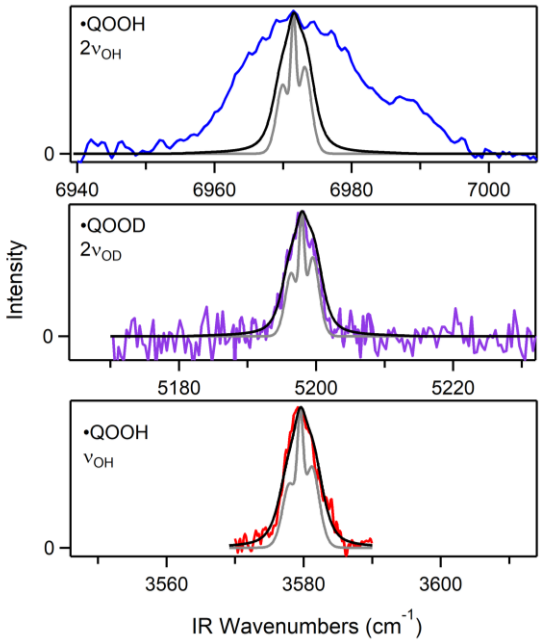

Figure 3. Comparison of IR spectral features observed by IR action spectroscopy with OH/D LIF detection for the overtone OH stretch of •QOOH ($2\nu_{OH}$, 6971.5 cm^{-1}; top), fundamental OD stretch of •QOOD (ν_{OD}, 5198.1 cm^{-1}; middle), and fundamental OH stretch of •QOOH (ν_{OH}, 3579.5 cm^{-1}; bottom). The intensities are in arbitrary units. Simulated rotational band contours are overlaid on the experimental IR action spectra. Simulations are shown at rotational temperature of 10 K with laser linewidth (0.9 cm^{-1}, gray), and with added contribution from homogenous broadening (1.7 cm^{-1}, black). Homogenous broadening is primarily attributed to rapid (ca. 3 ps) intramolecular vibrational energy redistribution (IVR), although some power broadening cannot be excluded. Simulations use computed rotational constants for •QOOH1 (*A*: 4.62 GHz, *B*: 2.87 GHz, and *C*: 2.80 GHz) and •QOOD1 (*A*: 4.59 GHz, *B*: 2.79 GHz, and *C*: 2.73 GHz) and transition types from VPT2 calculations.[7] The top and bottom panels are reproduced from Hansen et al., *J. Chem. Phys.*, 2022, **156**, 014301 with permission of AIP Publishing.

The outlier appears to be the •QOOH ($2\nu_{OH}$) feature at 6971.5 cm^{-1}, which has a significantly greater span (ca. 30 cm^{-1}) than the rotational band contours observed for other •QOOH/D transitions or simulations. As discussed recently,[7] the breadth of the $2\nu_{OH}$ feature likely arises from coupling with nearby •QOOH state(s) with three (or more) quanta of excitation through cubic terms in the expansion of the potential, which are not considered in VPT2 as implemented in Gaussian.[30] An extended VPT2 treatment[37] has identified many three quantum states in close proximity of $2\nu_{OH}$,[7] although not the specific state(s) that would give rise to an accidental degeneracy with $2\nu_{OH}$. We note that $2\nu_{OH}$ excitation prepares •QOOH above the TS barrier to ROO• (19.3 kcal mol^{-1}).[6, 13] This could potentially introduce

anharmonicities in the •QOOH potential that are not captured by the VPT2 calculations.[7] The unexpected breadth of the $2\nu_{OH}$ feature is not fully understood and warrants further study.

An additional •QOOD feature was observed at 4534 cm^{-1} with OD LIF detection, ascribed to the $\nu_{CH_2} + \delta_{CH_2}$ combination band, which is precisely the same frequency as the analogous transition observed for •QOOH as shown in Figure S3 using a 100 ns pump-probe delay. Unfortunately, this feature is too weak for rotational band contour analysis, as had been found for the same transition of •QOOH.[7] Nor was this feature strong enough for a lifetime measurement. Other weak CH combination bands observed for •QOOH were not explored for •QOOD.

The unimolecular decay rate of •QOOD following IR activation on the $2\nu_{OD}$ transition at 5198.1 cm^{-1} was measured by varying the time delay between the IR pump and UV probe lasers. A temporal profile showing the rate of appearance of OD products is given in Figure 4. The temporal profile is fit using a dual exponential function that accounts for the rapid appearance of OD products $k(E)$, and slow decay as OD products move out of the probe laser volume, along with the temporal profiles of the IR pump and UV probe lasers (see SI). The resultant rate for OD production and associated •QOOD unimolecular decay rate $k(E)$ is $1.0 \pm 0.3 \times 10^8$ s^{-1} ($\tau = 9.8 \pm 3.0$ ns) with $\pm 1\sigma$ uncertainty derived from repeated measurements. For comparison, Figure 4 also shows the temporal profiles that yield the unimolecular decay rates (and associated lifetimes) for •QOOH ($2\nu_{OH}$) at 6971.5 cm^{-1} of $\geq 2.6 \pm 0.5 \times 10^6$ s^{-1} ($\leq 3.8 \pm 0.8$ ns, laser limited) and that for •QOOH (ν_{OH}) at 3579.5 cm^{-1} of $4.1 \pm 1.3 \times 10^6$ s^{-1} (247 ± 77 ns).[6]

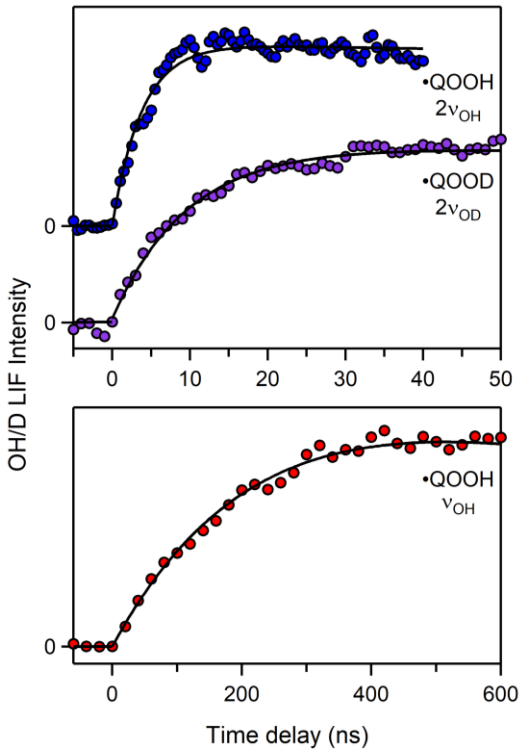

Figure 4. Representative time-resolved appearance profiles for OH or OD products following IR activation of •QOOH or •QOOD, respectively. Temporal profiles showing the appearance of OH/D radical products (points) following IR activation of •QOOH at 6971.5 cm^{-1} ($2\nu_{OH}$, blue) or •QOOD at 5198.1 cm^{-1} ($2\nu_{OD}$, purple) in the top panel, and •QOOH at 3579.5 cm^{-1} (ν_{OH}, red) in the bottom panel. The experimental •QOOH/D unimolecular decay rates (and corresponding OH/D risetimes) are: $\geq 2.6 \pm 0.5 \times 10^6$ s^{-1} ($\leq 3.8 \pm 0.8$ ns; laser-limited), $1.0 \pm 0.3 \times 10^8$ s^{-1} (9.8 ± 3.0 ns), and $4.1 \pm 1.3 \times 10^6$ s^{-1} (247 ± 77 ns). A much slower exponential decay originating from OH/D products moving out of the UV probe laser beam is derived from time profiles recorded on a longer timescale. The experimental time profiles are fit with a dual exponential function (black solid line) convoluted with the IR and UV pulse widths. The OH/D LIF intensities are in arbitrary units. The •QOOH $2\nu_{OH}$ and ν_{OH} time traces are reproduced with permission from Hansen et al., *Science*, 2021, **373**, 679-682 (2021). Copyright 2021 AAAS.

The energy-dependent unimolecular decay rates $k(E)$ for •QOOD are computed using statistical RRKM theory for comparison with experiment and prior investigation of •QOOH dissociation rates in the 3250 to 7500 cm^{-1} region.[6] The TS barrier leading to unimolecular dissociation increases slightly for •QOOD (10.5 kcal mol^{-1}) compared to •QOOH (10.3 kcal mol^{-1}) as a result of changes in the ZPE of the reactant and TS (Table S3) associated with the OH/D stretch, OOH/D bend, and COOH/D torsion (Table 1). Changes in these vibrations upon partial deuteration also affect the density of states of the reactant and tunneling-weighted sum of states at the TS. The imaginary frequency at the TS is unchanged (763*i* cm^{-1}), since tunneling involves heavy atom motion associated with simultaneous O-O bond elongation and C-O-O angle contraction along the reaction pathway to yield OD (or OH) and cyclic ether (DMEPOX) products.

The RRKM rates computed for •QOOD are shown in Figure 5 (Table S4) with tunneling (purple) and without tunneling (light gray). At 5200 cm^{-1}, the calculated rate with tunneling is 7.6×10^7 s^{-1} (τ = 13 ns), which is within ±1σ uncertainty of the experimentally observed rate. Tunneling increases the unimolecular dissociation rate significantly at energies in the vicinity of the TS barrier (10.5 kcal mol^{-1}), although the tunneling enhancement falls off with increasing energy. Specifically, tunneling is predicted to enhance the unimolecular decay rate of •QOOD by more than 7-fold at 3700 cm^{-1}, 40% at 5200 cm^{-1} and 15% at 7500 cm^{-1}. The corresponding experimental and computed RRKM rates for •QOOH are also shown in Figure 5 with (red) and without (dark gray) tunneling.[6] Again, tunneling significantly enhances the unimolecular decay rate of •QOOH at low energies in the vicinity of the TS barrier (10.3 kcal mol^{-1}), in accord with experimentally observed rates.[6]

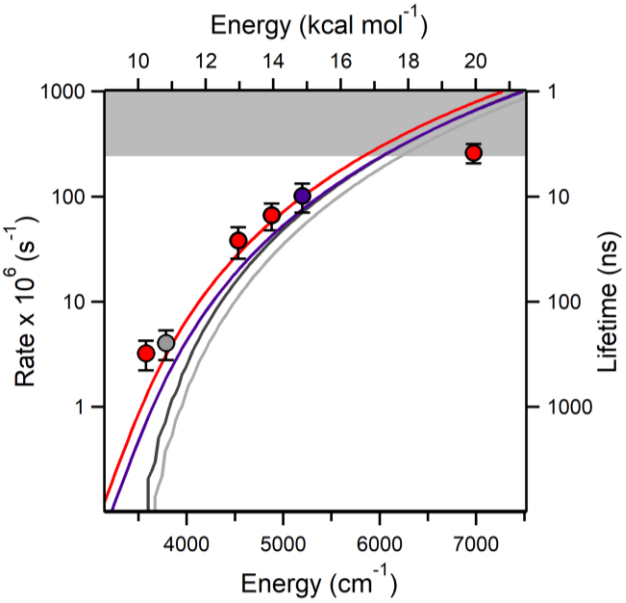

Figure 5. Rates and lifetimes (semi-log scale) for the unimolecular decay of •QOOH and •QOOD to OH/D and cyclic ether products. The experimental rates are given by the circles (•QOOD in purple and •QOOH in red and gray, the latter attributed to a higher energy conformer[6]) with error bars (±1σ) derived from repeated measurements. RRKM rates and lifetimes are calculated with tunneling (solid lines, •QOOD in purple and •QOOH in red) and without tunneling (solid lines, •QOOD in light gray and •QOOH in dark gray). The gray shaded region indicates rates limited by the experimental time resolution (4 ns).

The RRKM dissociation rate is predicted to be nearly two times faster for •QOOH than •QOOD at ca. 3700 cm^{-1}, where tunneling is significant. The more rapid RRKM rate for •QOOH than •QOOD at low energy is primarily due to the slightly higher TS barrier for •QOOD, which slows tunneling due to an increase in the volume of the inverted potential from the barrier top for •QOOD. At higher energies, the RRKM rate predicted for •QOOD approaches that for •QOOH. For example, the •QOOD decay rates at 5200 and 7500 cm^{-1} are only 30% and 20% slower than those for •QOOH, respectively. As the energy increases above the TS barrier, the importance of tunneling decreases and the density of reactant states

(Figure S4) primarily determines the relative rates. If the TS barrier for •QOOD is artificially set at 10.3 kcal mol^{-1}, the same as that for •QOOH, with vibrational frequencies unchanged, the unimolecular decay rates for •QOOD and •QOOH are nearly the same across the full energy range as shown in Figure S5.

The kinetic isotope effect (KIE), defined as k(•QOOH) / k(•QOOD), is predicted to decrease from 1.7 to 1.2 with increasing energy over the 3700 to 7500 cm^{-1} range. This small KIE demonstrates that the unimolecular dissociation of •QOOH/D to OH/D + cyclic ether products is not enhanced by light atom (H/D) tunneling associated with a bond to the isotopically labeled H/D atom being formed or broken. Rather, the slight change in unimolecular dissociation rate upon partial deuteration arises from a small increase in the TS barrier height due to ZPE effects. The significant tunneling enhancement in the unimolecular dissociation rate for •QOOH/D has been shown theoretically to originate from heavy atom motion involving simultaneous O-O elongation and C-O-O contraction along the reaction coordinate.[6]

Conclusions

The infrared spectroscopy and unimolecular dissociation dynamics of a prototypical hydroperoxylalkyl radical (•QOOH) are examined upon partial deuteration (–OOH/D) and compared with recent reports on •QOOH.[6, 7] The IR spectral feature and microcanonical unimolecular dissociation rate of the •$CH_2(CH_3)_2$COOD (•QOOD) radical are characterized upon vibrational activation of the overtone OD stretch ($2\nu_{OD}$) at 5198 cm^{-1}. The $2\nu_{OD}$ transition of •QOOD is shifted to significantly lower frequency than the $2\nu_{OH}$ transition of •QOOH at 6971 cm^{-1}, in very good accord with the calculated anharmonic frequencies (VPT2). The $\nu_{CH_2} + \delta_{HCH}$ combination band observed at 4534 cm^{-1} is essentially unchanged upon partial deuteration as expected theoretically. The observed spectral features expand the IR fingerprint of •QOOH/D and further validate the theoretical (VPT2) predictions.

The vibrational energy associated with •QOOD ($2\nu_{OD}$) excitation provides a new window for probing the energy-dependent unimolecular dissociation rates of •QOOH/D. The time-resolved appearance of OD products following vibrational activation of •QOOD at 5198 cm^{-1} yields a microcanonical dissociation rate $k(E)$ of $1.0 \pm 0.3 \times 10^8$ s^{-1} ($\tau = 9.8 \pm 3.0$ ns) with $\pm 1\sigma$ uncertainty. This expands the experimental observation of unimolecular decay rates for •QOOH/D. Complementary statistical RRKM calculations of the unimolecular dissociation rate for •QOOD at 5200 cm^{-1} including tunneling is 7.6×10^7 s^{-1} ($\tau = 13$ ns), which is within experiment uncertainty. Heavy-atom tunneling involving simultaneous O-O bond elongation and C-O-O angle contraction with associated imaginary frequency of 763i cm^{-1} increases the unimolecular dissociation rate predicted at this energy by 40%. The very good agreement of experimental and RRKM microcanonical rates with tunneling for •QOOD provide further validation of the TS barrier predicted from high level theory for a prototypical •QOOH radical, after accounting for small changes in ZPE upon partial deuteration. In addition, the analogous unimolecular decay rates for •QOOH and

•QOOD at similar energies, after accounting for small changes in ZPE, demonstrate that the heavy atom tunneling predicted for •QOOH/D is essentially unaffected by deuteration of the hydroperoxy (–OOH/D) group. Moreover, the very good agreement between experiment and theory for •QOOD further validates the overall interpretation of the observations.

Author Contributions

M.I.L. conceived the idea and designed the experimental research. S.C., T.B., and P.J.W. synthesized the precursor. T.B. and A.S.H. performed the experiments and analyzed the experimental data. A.S.H. and T.B. contributed to the spectroscopic calculations. A.S.H. carried out the kinetics calculations. S.J.K. conceptualized and developed the theoretical research. M.I.L. and S.J.K. supervised and guided the overall research. M.I.L wrote the paper with input from all authors.

Conflict of Interest

There are no conflicts of interest to declare.

Data Availability

The data that support the findings of this study are available within the article, its electronic supplementary information, and Zenodo (Ref. 38).

Acknowledgments

This research was primarily supported by the U.S. Department of Energy-Basic Energy Sciences under grant DE-FG02-87ER13792 (MIL). Partial equipment support was provided by the National Science Foundation under grant CHE-1955068 (MIL). This work utilized the Extreme Science and Engineering Discovery Environment (XSEDE), which is supported by the National Science Foundation grant number ACI-1548562 through the allocation TG-CHE190088. The contributions from SJK were supported by the U.S. Department of Energy (USDOE), Office of Basic Energy Sciences, Division of Chemical Sciences, Geosciences, and Biosciences under DOE Contract Number DE-AC02-06CH11357. ASH gratefully acknowledges support from the Carlsberg Foundation (CF18−0614) and the Independent Research Fund Denmark (9036−00016B). SC thanks the Natural Science Foundation of AnHui Province, China (2108085QB77) and PJW thanks the National Science Foundation (CHE1902509) for support.

References

1. D. R. Glowacki and M. J. Pilling, *ChemPhysChem*, 2010, **11**, 3836-3843.
2. D. L. Osborn, *Annu. Rev. Phys. Chem.*, 2017, **68**, 233-260.
3. M. J. Goldman, W. H. Green and J. H. Kroll, *J. Phys. Chem. A*, 2021, **125**, 10303-10314.
4. J. J. Orlando and G. S. Tyndall, *Chem. Soc. Rev.*, 2012, **41**, 6294-6317.
5. J. D. Savee, E. Papajak, B. Rotavera, H. Huang, A. J. Eskola, O. Welz, L. Sheps, C. A. Taatjes, J. Zádor and D. L. Osborn, *Science*, 2015, **347**, 643.
6. A. S. Hansen, T. Bhagde, K. B. Moore, D. R. Moberg, A. W. Jasper, Y. Georgievskii, M. F. Vansco, S. J. Klippenstein and M. I. Lester, *Science*, 2021, **373**, 679-682.
7. A. S. Hansen, T. Bhagde, Y. Qian, A. Cavazos, R. M. Huchmala, M. A. Boyer, C. F. Gavin-Hanner, S. J. Klippenstein, A. B. McCoy and M. I. Lester, *J. Chem. Phys.*, 2022, **156**, 014301.
8. J. Zádor, C. A. Taatjes and R. X. Fernandes, *Prog. Energy Combust. Sci.*, 2011, **37**, 371-421.
9. J. D. Crounse, L. B. Nielsen, S. Jørgensen, H. G. Kjaergaard and P. O. Wennberg, *J. Phys. Chem. Lett.*, 2013, **4**, 3513-3520.
10. J. Peeters, J.-F. Müller, T. Stavrakou and V. S. Nguyen, *J. Phys. Chem. A*, 2014, **118**, 8625-8643.
11. M. Ehn, J. A. Thornton, E. Kleist, M. Sipilä, H. Junninen, I. Pullinen, M. Springer, F. Rubach, R. Tillmann, B. Lee, F. Lopez-Hilfiker, S. Andres, I.-H. Acir, M. Rissanen, T. Jokinen, S. Schobesberger, J. Kangasluoma, J. Kontkanen, T. Nieminen, T. Kurtén, L. B. Nielsen, S. Jørgensen, H. G. Kjaergaard, M. Canagaratna, M. D. Maso, T. Berndt, T. Petäjä, A. Wahner, V.-M. Kerminen, M. Kulmala, D. R. Worsnop, J. Wildt and T. F. Mentel, *Nature*, 2014, **506**, 476.
12. F. Bianchi, T. Kurtén, M. Riva, C. Mohr, M. P. Rissanen, P. Roldin, T. Berndt, J. D. Crounse, P. O. Wennberg, T. F. Mentel, J. Wildt, H. Junninen, T. Jokinen, M. Kulmala, D. R. Worsnop, J. A. Thornton, N. Donahue, H. G. Kjaergaard and M. Ehn, *Chem. Rev.*, 2019, **119**, 3472-3509.
13. K. B. Moore, J. M. Turney and H. F. Schaefer, *J. Chem. Phys.*, 2017, **146**, 194304.
14. J. Zádor, H. Huang, O. Welz, J. Zetterberg, D. L. Osborn and C. A. Taatjes, *Phys. Chem. Chem. Phys.*, 2013, **15**, 10753-10760.
15. C. A. Whelan, M. A. Blitz, R. Shannon, L. Onel, J. P. Lockhart, P. W. Seakins and D. Stone, *J. Phys. Chem. A*, 2019, **123**, 10254-10262.
16. M. Baasandorj, D. K. Papanastasiou, R. K. Talukdar, A. S. Hasson and J. B. Burkholder, *Phys. Chem. Chem. Phys.*, 2010, **12**, 12101-12111.
17. A. S. Hansen, R. M. Huchmala, E. Vogt, M. A. Boyer, T. Bhagde, M. F. Vansco, C. V. Jensen, A. Kjærsgaard, H. G. Kjaergaard, A. B. McCoy and M. I. Lester, *J. Chem. Phys.*, 2021, **154**, 164306.
18. E. Vogt, R. M. Huchmala, C. V. Jensen, M. A. Boyer, J. Wallberg, A. S. Hansen, A. Kjærsgaard, M. I. Lester, A. B. McCoy and H. G. Kjaergaard, *J. Chem. Phys.*, 2021, **154**, 164307.
19. Y. Fang, F. Liu, V. P. Barber, S. J. Klippenstein, A. B. McCoy and M. I. Lester, *J. Chem. Phys.*, 2016, **144**, 061102.
20. M. I. Lester and S. J. Klippenstein, *Acc. Chem. Res.*, 2018, **51**, 978-985.
21. T. A. Stephenson and M. I. Lester, *Int. Rev. Phys. Chem.*, 2020, **39**, 1-33.
22. T. Baer and W. L. Hase, *Unimolecular reaction dynamics theory and experiments*, Oxford University Press, New York, 1996.
23. A. W. Jasper, K. M. Pelzer, J. A. Miller, E. Kamarchik, L. B. Harding and S. J. Klippenstein, *Science*, 2014, **346**, 1212-1215.
24. S. M. Saunders, M. E. Jenkin, R. G. Derwent and M. J. Pilling, *Atmos. Chem. Phys.*, 2003, **3**, 161-180.
25. H. J. Curran, *Proc. Combust. Inst.*, 2019, **37**, 57-81.
26. J. Bugler, J. Power and H. J. Curran, *Proc. Combust. Inst.*, 2017, **36**, 161-167.
27. F. Liu, J. M. Beames, A. S. Petit, A. B. McCoy and M. I. Lester, *Science*, 2014, **345**, 1596-1598.
28. F. Liu, J. M. Beames and M. I. Lester, *J. Chem. Phys.*, 2014, **141**, 234312.
29. H.-J. Werner, P. J. Knowles, G. Knizia, F. R. Manby, M. Schütz, P. Celani, W. Györffy, D. Kats, T. Korona, R. Lindh, A. Mitrushenkov, G. Rauhut, K. R. Shamasundar, T. B. Adler, R. D. Amos, A. Bernhardsson, A. Berning, D. L. Cooper, M. J. O. Deegan, A. J. Dobbyn, F. Eckert, E. Goll,

C. Hampel, A. Hesselmann, G. Hetzer, T. Hrenar, G. Jansen, C. Köppl, Y. Liu, A. W. Lloyd, R. A. Mata, A. J. May, S. J. McNicholas, W. Meyer, M. E. Mura, A. Nicklaß, D. P. O'Neill, P. Palmieri, D. Peng, K. Pflüger, R. Pitzer, M. Reiher, T. Shiozaki, H. Stoll, A. J. Stone, R. Tarroni, T. Thorsteinsson, M. Wang and M. Welborn, MOLPRO 2020.1, A package of ab initio programs, see www.molpro.net, 2020.

30. M. J. Frisch, G. W. Trucks, H. B. Schlegel, G. E. Scuseria, M. A. Robb, J. R. Cheeseman, G. Scalmani, V. Barone, G. A. Petersson, H. Nakatsuji, X. Li, M. Caricato, A. V. Marenich, J. Bloino, B. G. Janesko, R. Gomperts, B. Mennucci, H. P. Hratchian, J. V. Ortiz, A. F. Izmaylov, J. L. Sonnenberg, D. Williams-Young, F. Ding, F. Lipparini, F. Egidi, J. Goings, B. Peng, A. Petrone, T. Henderson, D. Ranasinghe, V. G. Zakrzewski, J. Gao, N. Rega, G. Zheng, W. Liang, M. Hada, M. Ehara, K. Toyota, R. Fukuda, J. Hasegawa, M. Ishida, T. Nakajima, Y. Honda, O. Kitao, H. Nakai, T. Vreven, K. Throssell, J. J. A. Montgomery, J. E. Peralta, F. Ogliaro, M. J. Bearpark, J. J. Heyd, E. N. Brothers, K. N. Kudin, V. N. Staroverov, T. A. Keith, R. Kobayashi, J. Normand, K. Raghavachari, A. P. Rendell, J. C. Burant, S. S. Iyengar, J. Tomasi, M. Cossi, J. M. Millam, M. Klene, C. Adamo, R. Cammi, J. W. Ochterski, R. L. Martin, K. Morokuma, O. Farkas, J. B. Foresman and D. J. Fox, Gaussian 16 Rev. A.03, Gaussian, Inc., Wallingford CT, 2016.
31. J. Towns, T. Cockerill, M. Dahan, I. Foster, K. Gaither, A. Grimshaw, V. Hazlewood, S. Lathrop, D. Lifka, G. D. Peterson, R. Roskies, J. R. Scott and N. Wilkens-Diehr, *Comput. Sci. Eng.*, 2014, **16**, 62-74.
32. S. J. Klippenstein, L. B. Harding and B. Ruscic, *J. Phys. Chem. A*, 2017, **121**, 6580-6602.
33. Y. Georgievskii and S. J. Klippenstein, MESS, 2020.1.24, MESS Master Equation System Solver available at GitHub.com/Auto-Mech, 2020.
34. M. D. Likar, J. E. Baggott and F. F. Crim, *J. Chem. Phys.*, 1989, **90**, 6266-6274.
35. R. D. Bach and H. B. Schlegel, *J. Phys. Chem. A*, 2020, **124**, 4742-4751.
36. PGOPHER, A Program for simulating rotational structure, C. M. Western, University of Bristol, http://pgopher.chm.bris.ac.uk.
37. M. A. Boyer and A. B. McCoy, *Zenodo*, 2021, DOI: https://doi.org/10.5281/zenodo.5563090.
38. T. Bhagde, A. S. Hansen, S. Chen, P. J. Walsh, S. J. Klippenstein and M. I. Lester, *Zenodo*, 2021, DOI: https://doi.org/10.5281/zenodo.5767557.